VOL.39 Nº1 2022
https://doi.org/10.22491/IMECTA.10841.en

A study of the lift and drag forces according to the pressure distribution in aerodynamic bodies

Daniel M Carvalho*, Victor Santoro Santiago*
Instituto Militar de Engenharia. Seção de Engenharia Mecânica, Rio de Janeiro,
Praça General Tibúrcio, 80 – Urca, CEP: 22290-270, Rio de Janeiro, Brasil
***daniel.carvalho@ime.eb.br; *santoro@ime.eb.br**

ABSTRACT: This study analyzes the effects of a lifting surface geometry in the calculation of its induced drag. For this purpose, we simulated a flow around a 3D airfoil with bell-shaped pressure distribution. Then, we compared the results of the efforts and yaw moment for different angles of attack with those traditionally found by elliptical pressure distribution, proving the emergence of the proverse yaw with a consequent induced drag decreasing.

KEYWORDS: Pressure distribution, lifting surfaces, induced drag.

RESUMO: O presente artigo buscou analisar os efeitos da geometria de uma superfície de sustentação no cálculo de seu arrasto induzido. Para tal, foi simulado o escoamento ao redor de um aerofólio 3D, o qual impõe uma distribuição de pressão em forma de sino. Os resultados dos esforços e do momento de guinada resultantes para diversos ângulos de ataque foram então comparados aos tradicionalmente obtidos por uma distribuição de pressão elíptica, comprovando o surgimento da guinada proversa com consequente diminuição do arrasto induzido.

PALAVRAS-CHAVE: Distribuição de pressão, superfícies de sustentação, arrasto induzido.

1. Introduction

Lifting and control surfaces are used in several engineering fields, such as aircraft, flow machines, missiles and rockets. However, the forces that originate lift also generate a force opposite to the movement, known as drag, or, more precisely, induced drag. This force is responsible for about 40% of the total drag on the body, and, at low speed, this number becomes even higher, reaching 90% [1].

Thus, this study analyzes the influence of the wing geometry on the induced drag production. To that end, we will address the bell-shaped pressure distribution proposed by Prandtl. This format is based on the model used in Bower's [2], and it will be developed in SOLIDWORKS™ and simulated in ANSYS Fluent™, since both software packages meet the complexities required by the project.

We will also assess the yaw moment and verify the existence of the reverse yaw (proverse yaw) for the bell-shaped pressure distribution model.

2. Theoretical framework

We describe some physical principles involved, and the theories they support.

2.1 Aerodynamic forces

For Araújo [3], the relative movement of a fluid causes pressure distribution changes around the body, besides causing shear stress on the surface. If added together, these effects give rise to the aerodynamic forces known as lift and drag.

2.1.1 Lift

Lift, as mentioned, is one of the forces generated by the relative movement between fluid and body. Its magnitude is directly proportional to the air density (ρ), wing surface area (A), and square of the relative flow velocity (V), as equation 1 shows below (Abbot [4]).

$$F_L = C_L \frac{\rho V^2}{2} A \qquad (1)$$

Where C_L is the lift coefficient, found according to the aerodynamic profile model, the Reynolds number and the angle of attack. It represents the profile efficiency in generating lift force (Ribeiro [5]).

2.1.2 Drag

Drag, as mentioned, is the force in the flow direction. It originates from the surface friction forces (viscous origin), the pressure forces, and the lift force (induced drag).

Besides these three drag forces, there is one more when it comes to supersonic speed, in which shock waves interfere in the movement. However, since this study is restricted only to subsonic speed, we will not explore this effect.

2.1.2.1 Friction drag

Friction drag comes from the existence of a boundary layer, which is the region adjacent to a solid surface where there are viscous stresses as opposed to the free current, and where these viscous stresses are negligible [6].

According to [6], the drag force relative to surface friction can be estimated by:

$$F_D = \int \tau_w dA \quad (2)$$

Where A is the total surface area in contact with the fluid and τ_w is the shear stress due to the boundary layer.

2.1.2.2 Form or pressure drag

Form or pressure drag is related to the body geometry, which can cause a pressure difference between the leading edge and the trailing edge, the ultimately responsible for the formation of the viscous flow [6]. Its magnitude is expressed by:

$$F_p = \int p dA \quad (3)$$

Where **p** is the pressure on the surface.

2.1.2.3 Induced drag

In bodies that generate lift, induced drag emerges related to the pressure difference between the top and bottom of the wings. The air in the lower surface tends to flow to the upper surface, inducing an eddy at the wing tip and generating the so-called wingtip vortices, as illustrated in **Figure 1**. This phenomenon is one of the main causes of the the formation of the viscous flow that causes resistance to the body advance [6].

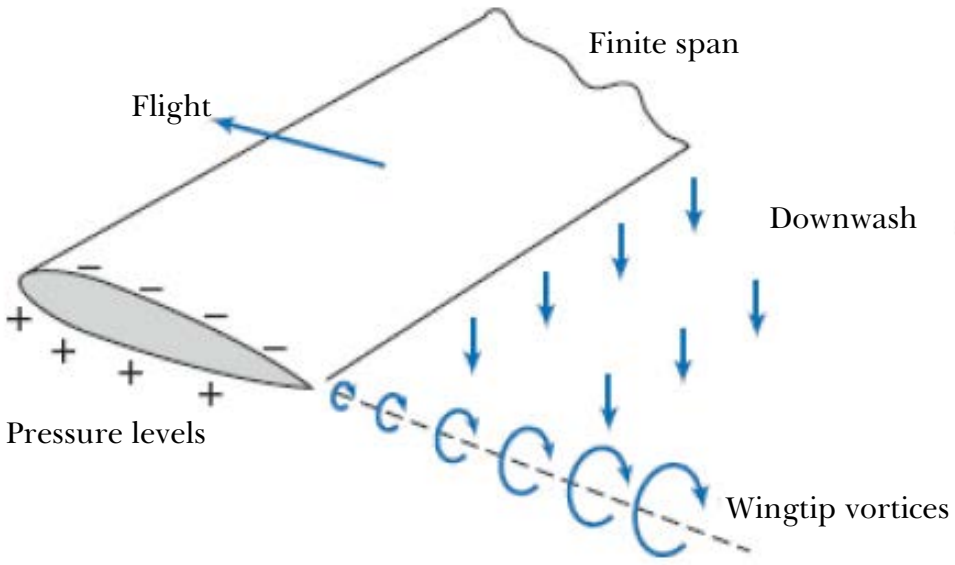

Fig. 1 - Wingtip vortices. Source: [6].

For Prandtl, the induced drag coefficient ($C_{D,i}$) is related to the lift coefficient and the shape aspect ratio [7], which reveals how dependent this drag is on the lift.

$$C_{D,i} = \frac{C_L^2}{\Pi e AR} \tag{4}$$

Where C_L is the lift coefficient, AR is the shape aspect ratio, is the efficiency factor.

$$F_D = C_D \frac{\rho V^2}{2} A \tag{5}$$

$$C_D = C_{D,i} + C_{D0} \tag{6}$$

Where C_{D0} is the parasite drag coefficient, resulting from the sum of the form drag and the friction drag, found experimentally.

2.2 Aerodynamic moments

We can consider these forces applied in a single point called aerodynamic center, and, depending on the angle of attack, a moment will appear around this point, which is given by

$$M = C_M \frac{\rho V^2}{2} LA \tag{7}$$

Where L is a reference length and C_M is the aerodynamic moment coefficient, which is also found experimentally.

This moment, when decomposed in the three main axes, will generate three characteristic aircraft rotations, which are rolling, yaw and pitch.

2.3 Prandtl's classical theory

Prandtl developed his theory between 1911 and 1918, using existing knowledge related to vortex filaments, which play an important role in the synthesis of complex flows. His premise was that the circulation intensity should not vary along the wing. However, observations showed that this fact is false for a finite wings. Thus, Prandtl suggested changing the wing shape, overlapping certain vortex filaments with different circulation intensity. As **Figure 2** shows [7].

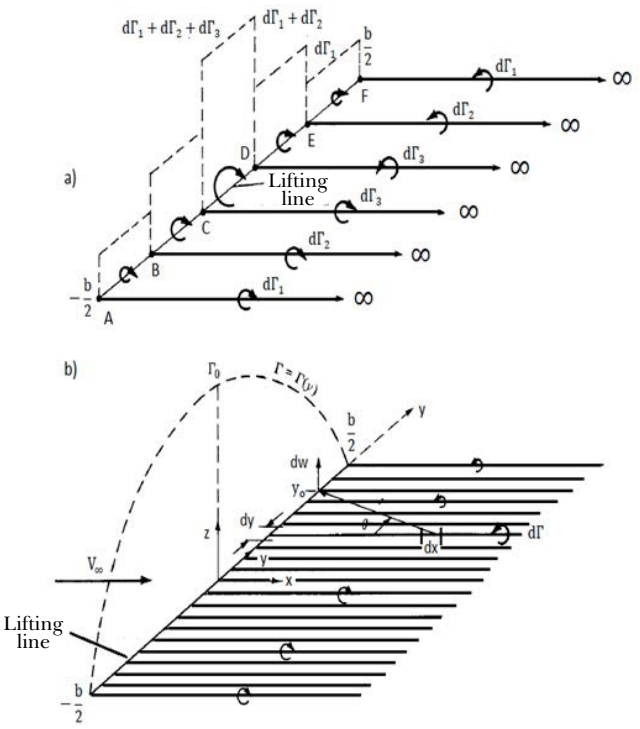

Fig. 2 - Overlap of numbers, finite (a) and infinite (b), of vortex filaments along the lifting line. Source: adapted from [7].

Free vortices are responsible for the emergence of the induced velocity w along the axis of the wing perpendicular to the lifting line. We find this velocity, at y_0, by the contribution of all free vortices, as shown in Equation 8:

$$w(y_0) = \frac{-1}{4\pi} \int_{-b/2}^{b/2} \frac{\left(\frac{d\Gamma}{dy}\right) dy}{y_0 - y} \tag{8}$$

Where b is the wingspan and y_0 is a point along the lifting line.

Since the undisturbed flow velocity, V_∞, is usually much higher than the descending component, w, the induced angle α_i takes a relatively small value. Thus, we can simplify the estimating of the induced angle by the following form:

$$\alpha_i(y_P) = -\frac{w(y_P)}{V_\infty} \tag{9}$$

The Kutta-Joukowski theory predicts that the lift distribution (L') is related to circulation, according to Equation 10:

$$L' = \rho V_\infty \Gamma(y_P) \tag{10}$$

Thus, considering this theory, the definition of the lift coefficient, and the concept of effective angle of attack, which is the angle between the chord and the relative flow, we meet the fundamental equation of Prandtl's lifting-line theory, represented by:

$$\alpha(y_0) = \frac{2\Gamma(y_0)}{\alpha_0 V_\infty c(y_0)} + \alpha_{L=0} + \frac{1}{4\pi V_\infty}\int_{-b/2}^{b/2} \frac{\left(\frac{d\Gamma}{dy}\right)dy}{y_0 - y} \tag{11}$$

Where $\Gamma(y)$ is the circulation intensity, α_0 is the lift-curve slope, $c(y_0)$ is the chord on $y=y_0$ and $\alpha_{L=0}$ is the zero lift angle of attack.

2.3.1 Elliptical pressure distribution

The elliptical distribution has the following circulation intensity:

$$\Gamma(y) = \Gamma(y_0)\sqrt{1-\left(\frac{2y}{b}\right)^2} \tag{12}$$

Therefore, Equations 8 and 9 result in the following induced angle:

$$\alpha_i = \frac{AC_L}{\pi b^2} \tag{13}$$

For the induced drag coefficient [7]:

$$C_{D,i} = \frac{2}{V_\infty A}\int_{-b/2}^{b/2} \Gamma(y)\alpha_i(y)dy \tag{14}$$

Solving:

$$C_{D,i} = \frac{AC_L^2}{\pi b^2} \tag{15}$$

Therefore, for the drag force:

$$F_{Di} = \frac{AC_L^2}{\pi b^2}\left(\frac{\rho V^2}{2}A\right) \tag{16}$$

As a result, an elliptical lift geometry can not solely and freely develop lift without paying a price, which will be the induced drag.

The relationship between circulation and pressure distribution, and the relationship between circulation and body geometry are interesting. According to Equation 10, the pressure distribution is directly related to the circulation. Thus, as the circulation is elliptical, so will the pressure distribution.

Without twist in the geometry, or torsion along the wing length, both α and $\alpha_{L=0}$ will be constants. By the concept of effective angle and the Kutta-Jukovski theory, we found the following equation for the relationship between circulation and body geometry:

$$c(y) = \frac{L'(y)}{c_L \frac{\rho V_\infty^2}{2}} \tag{17}$$

As $c(y)$ is directly proportional to the pressure distribution with an elliptical shape, the chord varies elliptically along its length, as **Figure 3** shows.

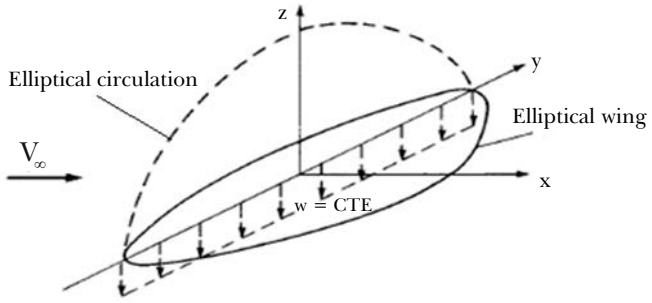

Fig. 3 - Elliptical wing. Source: [7].

2.3.2 Bell-shaped pressure distribution

Prandtl, in 1933, and Horten, in 1935, developed works about geometry with minimal induced drag. The first, correcting his 1922 theory, estimated the total induced drag force for a wing which pressure distribution is bell-shaped, and concluded that this new distribution is more efficient than the elliptical pressure distribution when reducing induced drag. However, he did not assess the distribution of this force around the wing length and failed in his implication. Thus, Horten, in 1935, become the responsible for estimating this force distribution, concluding in 1950 that this distribution may present a singularity. What Prandtl failed and Horten believed to exist is the reverse yaw [2].

The solution for the bell-shaped circulation distribution, developed by Prandtl in 1933, was:

$$\Gamma(0) = \left(1 - 0^2\right)^{\frac{3}{2}} \quad (18)$$

Meeting the downwash of:

$$w(y) = \frac{3}{2}\left(y^2 - \frac{1}{2}\right) \quad (19)$$

Figure 4 shows the two Prandtl distributions, 1922 and 1933.

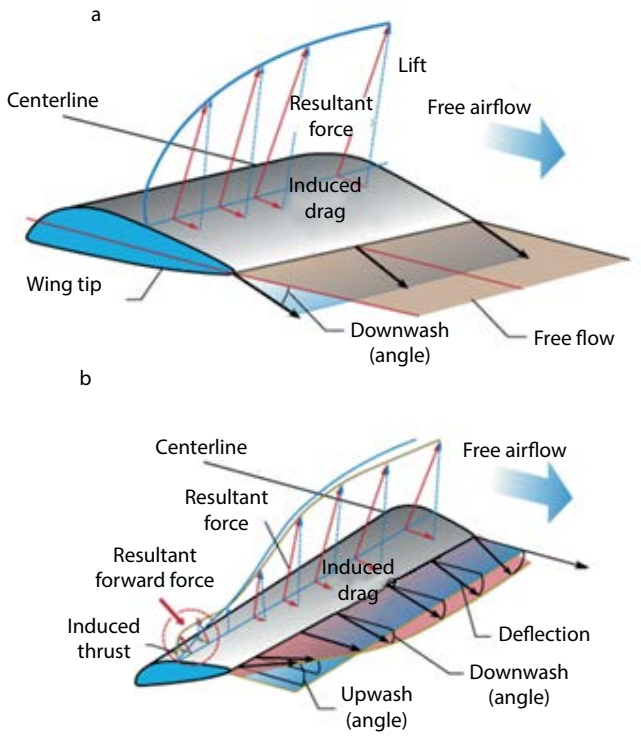

Fig. 4 - Prandtl explanation. Source: [2].

The elliptical pressure distribution shown in **Figure 4** (a) produces a constant induced drag resultant in the flow direction, according to the steady downwash along the wing length. On the other hand, **Figure 4** (b) shows the transition from downwash to upwash along the wing. The resulting lift force in this upwash region is tilted forward, and its horizontal component represents an induced thrust at the wing tip, explaining the emergence of the reverse yaw [2].

As a consequence, when adding a control surface (aileron or elevon) to generate a rolling moment on an elliptical wing, an external yaw moment is also produced, in opposition to the intended yaw, and for this reason it is called adverse yaw. In turn, a wing with bell-shaped pressure distribution would produce a moment that aids the control, once it contributes to the intended yaw and, for that reason, it is called reverse or proverse yaw. Thus, aircraft with elliptical pressure distribution need devices that aid the yaw, such as the horizontal rudder/stabilizer, a device that could be reduced or even dismissed in the bell-shaped pressure distribution model. The suppression of the rudder would also represent a weight and drag reduction in the aircraft as a whole.

3. Computational modeling

This chapter addresses the modeling of the bell-shaped pressure profile proposed by [2] and its control surface, the elevon, which will be added to it.

3.1 Bower's Wing

We made the modeling of this wing using data from [2], which provided the airfoils in coordinates. We inserted these coordinates into SOLIDWORKS™, resulting in the central and wing tip airfoil surfaces, as **Figure 5** shows. These surfaces have a distance of 1874.52 mm from each other.

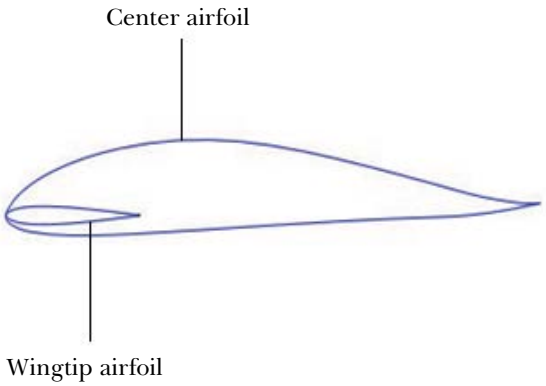

Fig. 5 - Side view. Source: Own authorship (2020).

We made twenty 93.73 mm divisions, equally spaced, from the wing root to its tip. In each subdivision, we placed planes containing the airfoil with the torsion angles described in [2]. In each plane, the airfoils were placed in a way that the wing gained

a sweep angle of 24° and a positive dihedral angle of 1.25°. **Figure 6** shows the result of this operation, and the intermediate planes are indicated.

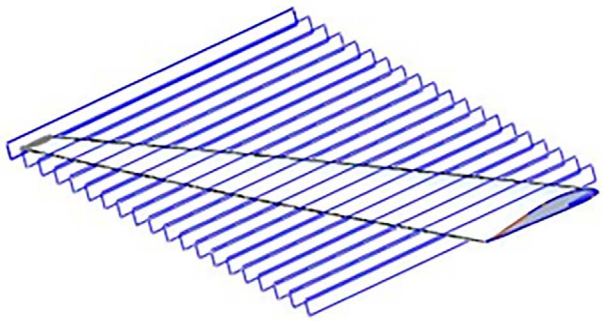

Fig. 6 - Wing division planes. Source: Own authorship (2020).

To be possible to add the control surface, we performed the following processes on the wings:

- Three base planes for the clipping, as **Figure 7** shows; and
- The intersection of these planes and the wing to cut out the elevon.

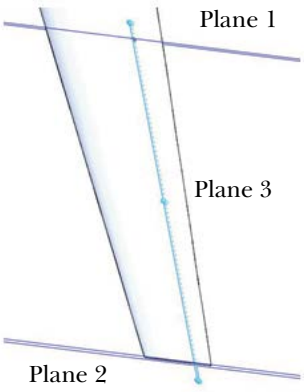

Fig. 7 - Clipping plans. Source: Own authorship (2020).

3.2 Control surface modeling

For the construction of this control surface, **Figure 8**, we performed the following procedures:

- Base planes identical to clipping planes;
- Intersection of planes and wing;
- Combination of intersections;
- Elevon structure detailing.

Fig. 8 - Elevon. Source: Own authorship (2020).

4. Results and discussion

The simulations allowed three possible settings for the elevon, −5°, 0° and 5°, all made in ANSYS Fluent™, using the SST model to describe the turbulence phenomenon. This model is widely used by the academic community due to its feature of combining advantages of two others K-ω and K-ε models.

4.1 Aerodynamic forces and moments

As a result of these simulations, we found the values of aerodynamic parameters present in **Table 1** for Bower's setting [2], with bell-shaped pressure distribution.

Tab. 1 - Results for Bower's model [2]

Parameter	Value		
Angle of attack –	−5°	0°	5°
Drag coeff. –	0.0096	0.0095	0.0108
Lift coeff. –	0.1567	0.1266	0.1123
Moment coeff. –	0.0105	0.0090	0.0107
Drag force (*N*) –	59.17	58.26	66.33
Lift force (*N*) –	960.61	775.98	688.21
Yaw moment (*N.m*) –	64.76	55.14	65.70

Comparing the values of drag coefficient (C_D) and drag force (F_D) between the settings (−5°, 0° and 5°), the drag force is lower with 0° angle of attack than with other angles, which is consistent with the theory, as the area of contact with air increases and, consequently, the

drag force becomes greater when inserting an angle in the elevon. The drag is higher to the 5° angle, since the torsion on the Bower's wing [2] makes these 5° higher at the tip in relation to the flow, which explains the higher drag. In turn, to the −5° angle, the flow may be lower in the sections near the wing tips.

The values of lift coefficient (C_L) and lift force (F_L) are also consistent with the theory, because the smaller the elevon angle, the greater the vertical force.

Regarding the yaw moment, −5° and 5° settings have greater moments than the 0° setting for both models, which can be explained by the presence of the control surface near the tip, generating, therefore, a higher drag and, consequently, a higher yaw moment. The resulting yaw moment will be −0.9413 N·m when the Bower's wing [2] is complete, with 5° at one edge and −5° at another, showing the emergence of the reverse yaw moment, and favoring the aircraft in curves. As expected, this phenomenon occurs only without the traditional elliptical pressure distribution, in which an adverse yaw moment of 14.2647 N·m occurs, value found in the simulation of a wing with an elliptical distribution model under the same conditions.

4.2 Bower's Wing

Besides the forces and coefficients estimated, we also analyzed the pressure distribution in six planes located at 0%, 40%, 60%, 80%, 90% and 100% of the wing root.

We present the results for the setting with Bower's −5° angle of attack [2] in **Figures 9** and **10**. The variation of the lift component occurred gradually along the wingspan, the downwash near the wing root changing to upwash near the wing tip, as **Figure 9** presents, showing the flow by the view of the entrance plane, where the red square indicates the center line of the vortex.

Figure 11 show a pressure distribution which resultant generates an upward force and a drag force in the opposite direction to the flow. **Figures 11** (d), (e) and (f) present the emergence of a significant pressure in the wing lower surface generated by the elevon, characterizing higher lift. Another result is the variation of the vertical component along the wingspan. In **Figures 11** (a) to (e), the lift component is in the same direction of the flow indicated by the arrow, and shows the emergence of the induced drag. However, in **Figure 11** (f), the lift component, represented by the pressure resultant, moves progressively to the opposite direction to the flow while gets closer to the wing tip, characterizing the thrust that generates the reverse yaw phenomenon.

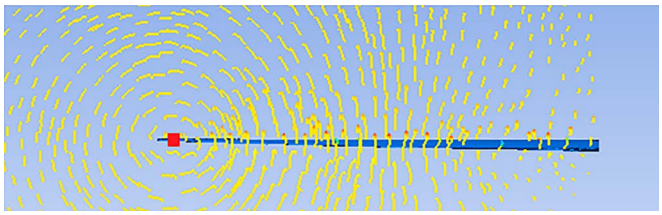

Fig. 9 - Airflow in the front view for −5° setting in Bower's model. Source: Own authorship (2020).

Figures 10 and **12** present the results for the setting with 0° angle of attack in [2]'s model: **Figures 12** (d) and (e) show the change from downwash to upwash, and **Figure 10**, shows the formation of a vortex between the wing tip and root. They are, therefore, in accordance with the literature. The point where the vortex occurs is closer to the wing root in relation to the −5° angle of attack simulation. This is because the elevon in this setting disfavors the induced thrust, as the normal on its surface is projected backwards, contributing to increase the drag on the wing tip.

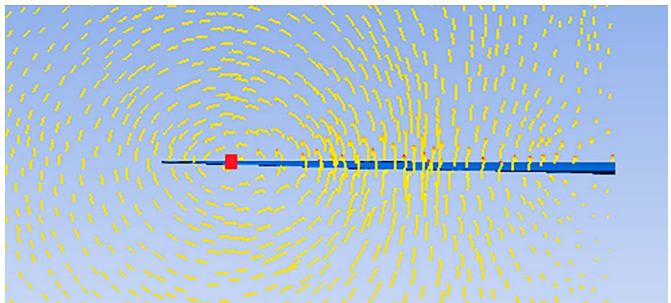

Fig. 10 - Airflow in the front view for −0° setting in Bower's model. Source: Own authorship (2020).

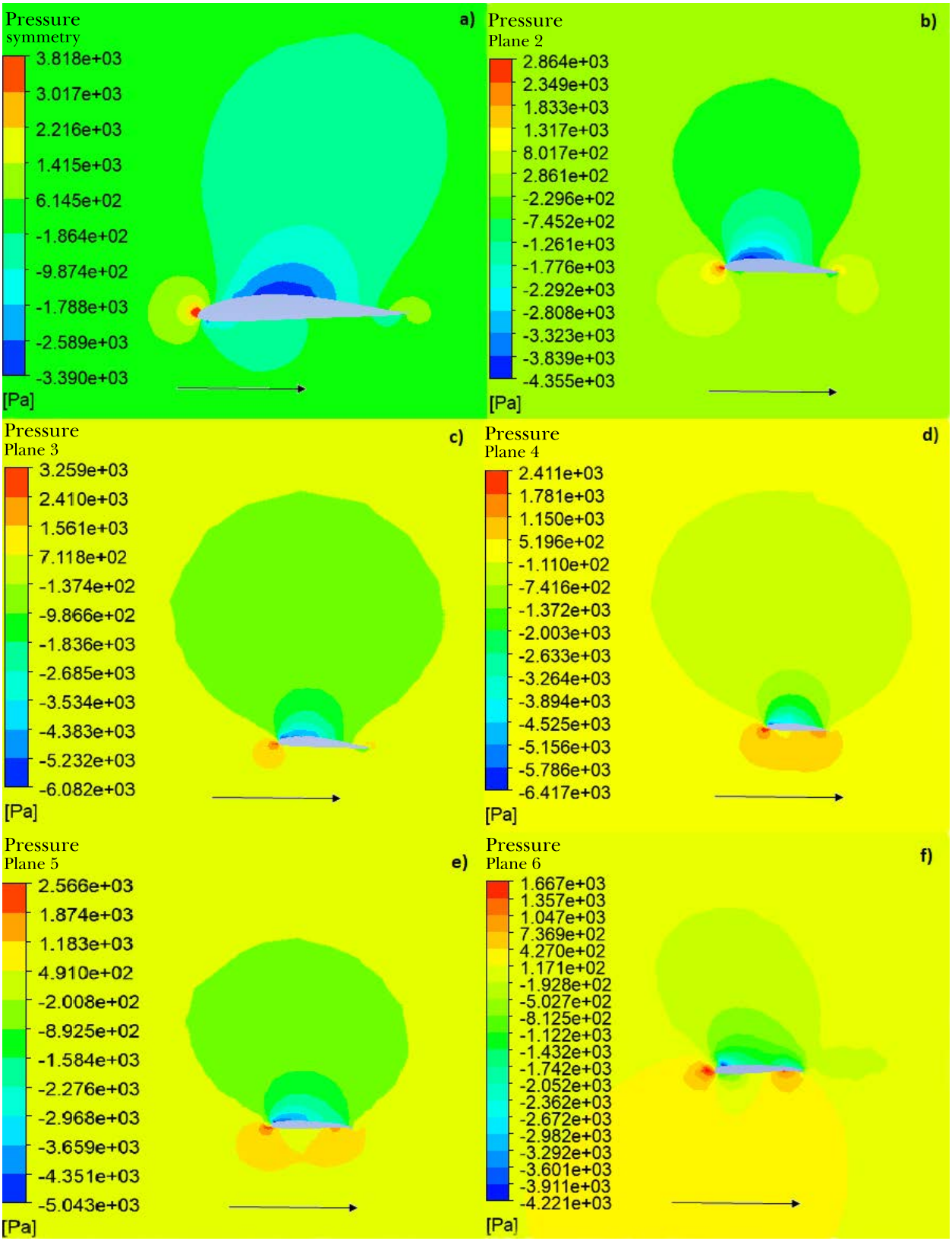

Fig. 11 - Pressure distribution for −5° setting in Bower's model in the planes: a) wing root; b) 40% of the wingspan; c) 60% of the wingspan; d) 80% of the wingspan; e) 90% of the wingspan; and f) wing tip. Source: Own authorship (2020).

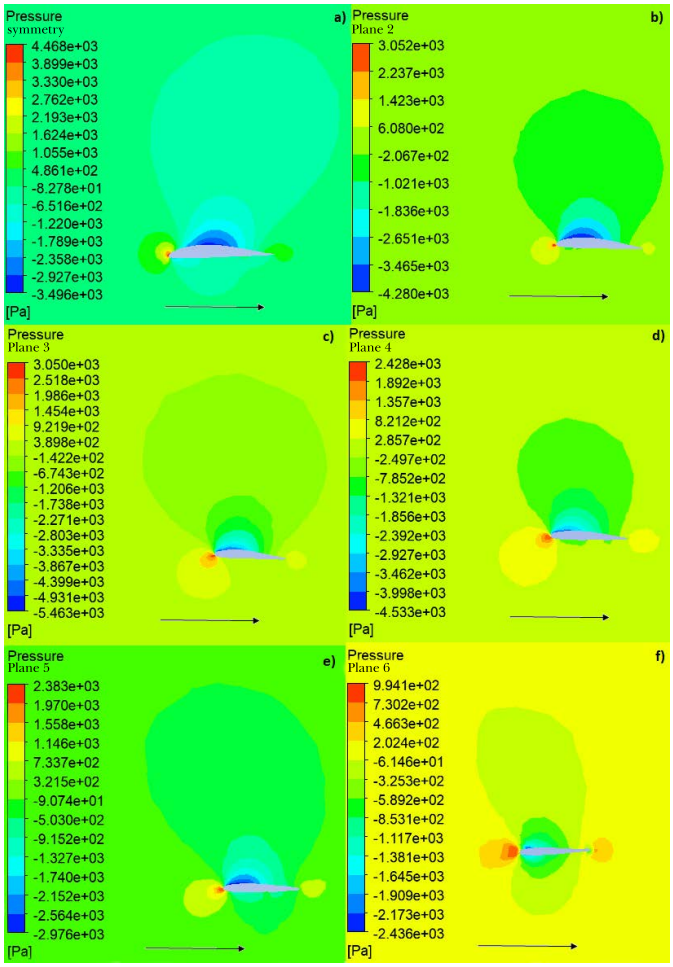

Fig. 12 - Pressure distribution for 0° setting in Bower's model in the planes: a) wing root; b) 40% of the wingspan; c) 60% of the wingspan; d) 80% of the wingspan; e) 90% of the wingspan; and f) wing tip. Source: Own authorship (2020).

For 5° angle of attack setting in [2]'s model, **Figures 13** and **14** present results similar to the previous ones, such as pressure distribution along the wingspan and the change from downwash to upwash in **Figures 14** (c) and (d), in addition to the formation of the vortex between the wing tip and root in **Figure 13**, which is, therefore, in accordance with the literature. The point where the vortex occurs is located more internally than in previous simulations. That is because the elevon in this setting favors the induced thrust, as the normal on its surface is projected forwards. **Figures 14** (d), (e) and (f) present the emergence of a significant pressure in the wing upper surface generated by the elevon, characterizing lower lift.

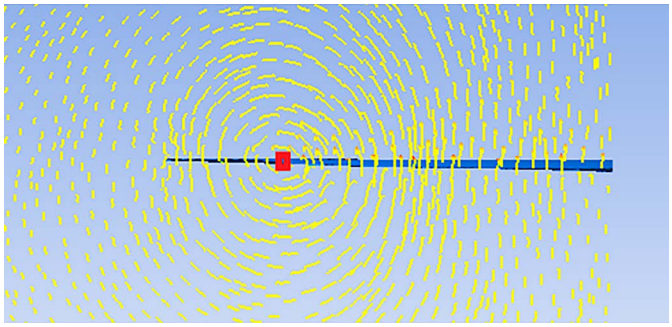

Fig. 13 - Airflow in the front view for 5° setting in Bower's model. Source: Own authorship (2020).

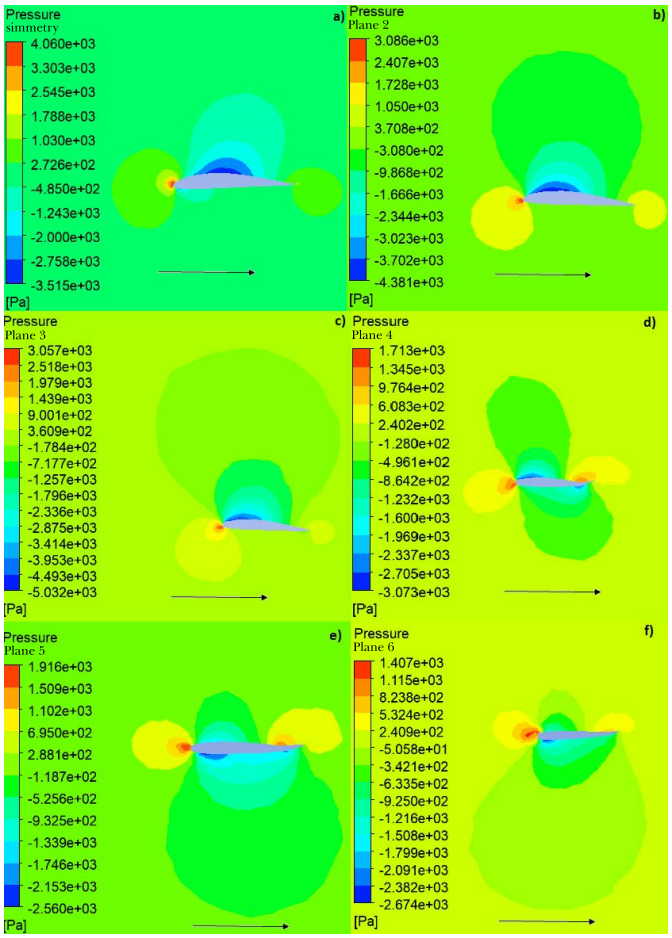

Fig. 14 - Pressure distribution for 5° setting in Bower's model in the planes: a) wing root; b) 40% of the wingspan; c) 60% of the wingspan; d) 80% of the wingspan; e) 90% of the wingspan; and f) wing tip. Source: Own authorship (2020).

5. Conclusion

The simulations performed in ANSYS Fluent™ were in accordance with Prandtl's theory and Bower's studies [2]. They show that the bell-shaped pressure

distribution model produces a yaw point that aids the aircraft control, which would allow, theoretically, the decrease or even suppression of rudders as a control surface. We also performed simulations of a wing with elliptical pressure distribution and found out results that allowed us to conclude that this model generates a high reverse yaw moment, indicating that rudders are indispensable in these cases.

Regarding aircraft lift, the bell-shaped pressure distribution model had better results, even with less material than the simulated elliptical model. This fact, added to the removal of the rudder, could decrease the total cost of manufacturing; however, the complex shape of its wing, with different torsion angles along its wingspan, hinders its construction and requires advanced engineering.

The elliptical model used for comparison is not unique. Its construction met some requirements that made it similar to Bower's [2], but other specifications were not met simultaneously due to the difference in these geometries.

References

[1] S BOWER, A.H, AND MURILLHO, O.J. **On wings of the Minimum induced Drag**: Spanload Implications for Aircraft and Birds, NASA/TP-2016-219072, 2016

[2] ARAÚJO, M.R.V. **Simulação e controle de veículo aéreo não tripulado Tail-Sitter. 126 f.** Dissertação (Mestrado em Sistema Mecatrônicos), Departamento de Engenharia Mecânica, Universidade de Brasília, Brasília, DF, 2007.

[3] ABBOTT, Ira H.; VON DOENHOFF, Albert E. **Theory of wing sections.** New York: Dover Publications, 1958. 705 p.

[4] RIBEIRO, Fernanda Alves. **Análise aerodinâmica de perfis de asa para aeronaves Experimentais tipo JN-1.** 2011. 95 f. Dissertação (Mestrado) - Curso de Engenharia Mecânica, Universidade Federal do Rio Grande do Norte, Natal, 2011.

[5] FOX, Robert W, MCDONALD, Alan T. **Introdução a mecânica dos fluidos**. 8 ed. Rio de Janeiro: Livros Técnicos e cientificos, 2001, 522 p.

[6] JHON D; ANDERSON JR. **Fundamentals of Aerodynamics.** 5. ed. New York: Mcgraw-hill, 2007. 1131 p.
(FR)